ISO observations of M8, the Lagoon nebula

Conference or Workshop Item

Star Formation with the Infrared Space Observatory
ASP Conference Series, Vol. 132, 1998
J. L. Yun, and R. Liseau, eds.

ISO Observations of M8, The Lagoon Nebula

Glenn J. White[1] B. Nisini[6], J.C.Correia[1], N.F.H.Tothill[1],M. Huldtgren[5], D.Lorenzetti[6] P. Saraceno[6], H.A.Smith[6], C.Ceccarelli[6], M.Burgdorf[6], M.J.Griffin[6], I.Furniss[6], W.Glencross[6], L.Spinoglio[6], H.E.Matthews[2], W.H.McCutcheon[3],and Mark J. McCaughrean[4]

Abstract. In this paper, IRAS, ISO, and molecular line observations of the M8 and M8E sources in the Lagoon Nebula are reported.

1. Introduction

M8, the Lagoon Nebula (NGC 6523), is one of the most prominent H II regions in the Galaxy. It has been studied over a wide range of wavelengths, as summarised by Lada *et al.* (1976), Elliot *et al.* (1984), Woodward *et al.* (1986) and Stecklum *et al.* (1995). The excitation of the central region is dominated by radiation from recently formed OB stars, especially the O7V star Herschel 36 (H 36). At far-IR wavelengths the region is dominated by emission from the bipolar Hourglass Nebula and the nearby compact source M8E.

2. Observations

The mm and submm wavelength data were obtained with the 15 metre James Clerk Maxwell Telescope (JCMT) in Hawaii; near-IR narrow-band ($\Delta\lambda/\lambda \sim 1\%$) observations of the He I 2^1P–2^1S ($\lambda 2.058\mu$m), H_2 v=1–0 S(1) ($\lambda 2.122\mu$m), and H I Brγ ($\lambda 2.166\mu$m) lines were made at the ESO/MPG 2.2 metre telescope on La Silla; a broad-band K′ frame was taken with the 3.9 m Anglo-Australian Telescope and mid-IR grating spectra were obtained with ISO's SWS and LWS spectrometers (see White *et al.* 1997 and the A&A ISO Special Issue for further details).

The Lagoon Nebula is a prominent H II region which contains the second most intense known CO molecular line source. The H II region is surrounded by several expanding shells of molecular material which have a total mass $\sim$ 1500

[1]Physics Department, Queen Mary & Westfield College, London E1 4NS

[2]Joint Astronomy Centre, Hilo and National Research Council of Canada

[3]University of British Columbia, Canada

[4]MPI für Radioastronomie, Bonn

[5]Stockholm Observatory, Sweden

[3]Other affiliations can be found in the A&A special ISO issue

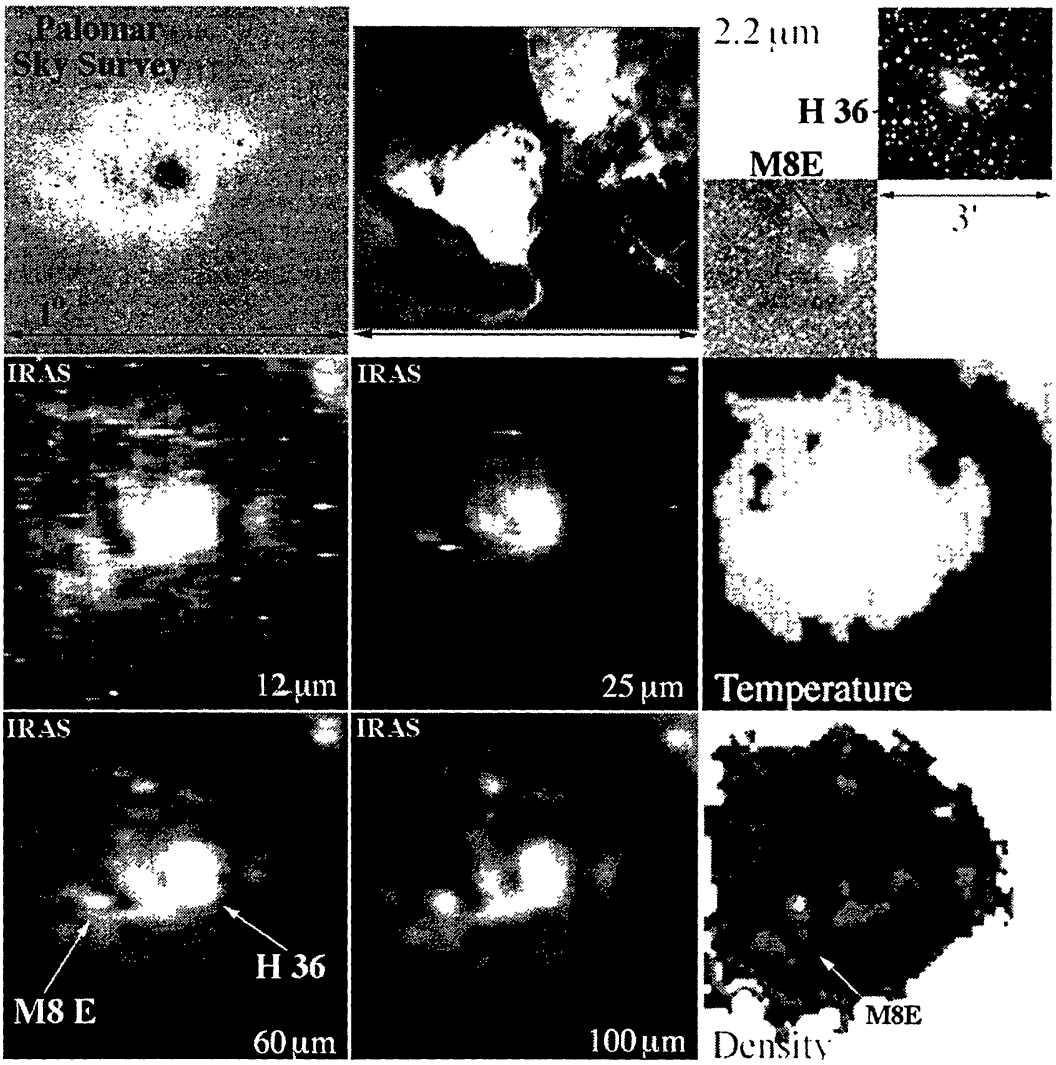

Figure 1. Composite of IRAS, optical and near-IR maps. All of maps cover a 1 square degree field, except the HST and 2.2 μm maps which cover about 9 square arcminutes each.

$M_\odot$. Numerous sites of triggered star-formation are found at the edges of the shells, rather like a pearl necklace strung out around the edge of the H II region. A composite view of the area around The Lagoon Nebula is shown in Figure 1.

CO molecular line emission at the position of H 36 is unusually intense, with peak temperatures $\sim$ 130 K. A composite of the various mm, near-IR and optical lines is shown in Figure 2.

As seen in Fig 2 c), the spatial distribution of the wings is quite complex; the red-shifted gas lies predominantly to the north, and blue-shifted gas dominates close to H 36 and the Hourglass Nebula. This traces the edge of a cavity surrounding H 36. From $C^{18}O$ observations, the mass of the core is $\sim$ 31 $M_\odot$ and the size is $\sim 0.2 \times 0.3$ pc. The integrated CO $J = 3 - 2$ emission peaks at H 36 and extends over a range of $\sim$ 20 km s^{-1}.

Spectra obtained with ISO towards M8E are shown in Fig 3.

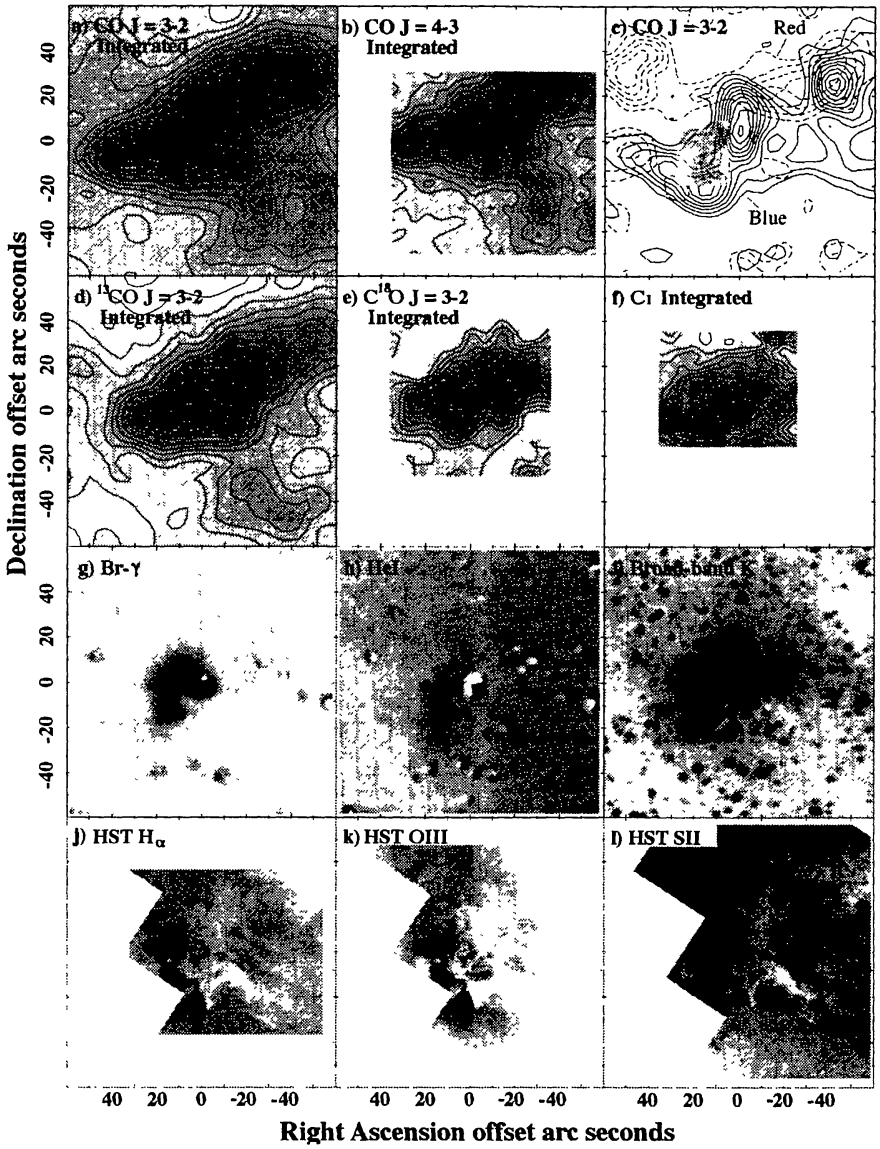

Figure 2. Maps and images of the Hourglass region: a) integrated CO $J = 3-2$ emission (2 – 23 km s^{-1}); b) integrated CO $J = 4-3$; c) high velocity blue (0 – 5.5 km s^{-1}) and red (15 – 20.5 km s^{-1}) emission, with the Hourglass Nebula indicated by the shaded region close to the centre; d) ^{13}CO $J = 3-2$ integrated emission; e) C^{18}O $J = 3-2$ integrated emission; f) CI integrated emission; g) continuum-subtracted Brγ ; h) continuum-subtracted He I. i) broad-band AAT K′ (used as the continuum to prepare g) and h)); j) HST Archive Hα ; k) HST Archive [O III]; l) HST [S II]. The contour values and ranges are listed in White *et al.* 1997. The (0,0) position is that of the exciting source H 36: $\alpha_{1950} = 18^h\ 00^m\ 36.3^s$, $\delta_{1950} =$ -24° 22′ 53″.

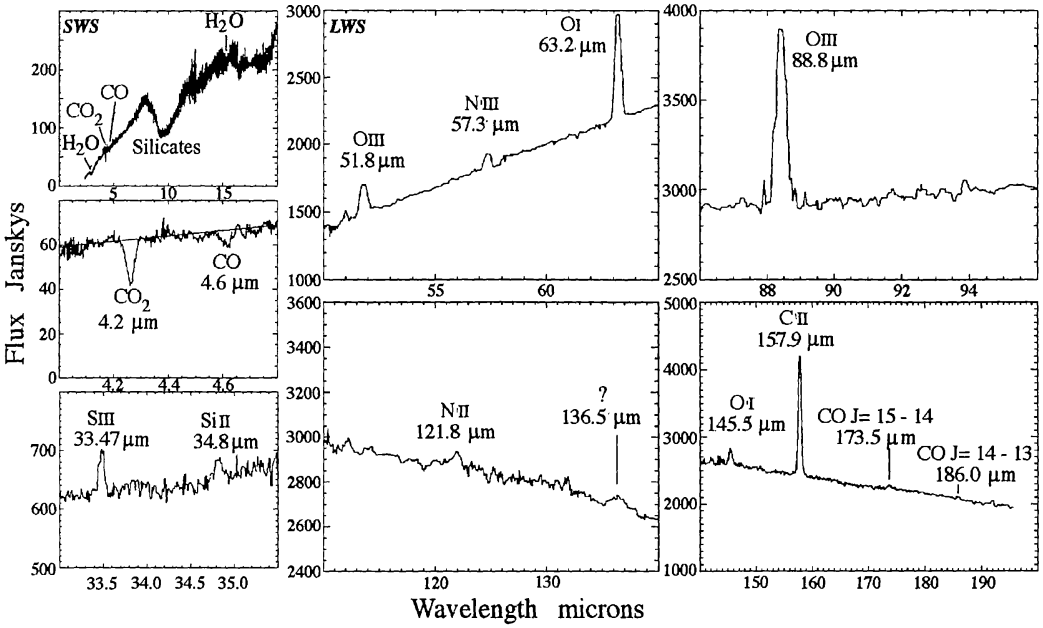

Figure 3. M8E SWS and LWS spectra. The SWS spectra contain a number of absorption lines due to CO, CO_2, and H_2O ices. The carrier of the emission feature at 136.5 μm cannot be identified; it is unlikely to be due to the $3_{30} - 3_{21}$ line of ortho H_2O, since other lower excitation water lines at 174 and 179 μm are not seen in the LWS spectra

M8E is the compact core seen in Figure 1 lying east of H 36. An analysis of the ISO LWS lines, and comparison with a nearby 'off-source' reference spectrum suggests that most of the lines seen in the LWS spectrum originate in a nearby, previously known, compact H II region. The fluxes of the [O I](63), [O I](145) and [C II](158) lines are respectively 1.5 10^{-17}, 1.2 10^{-18} and 7.6 10^{-18} W cm^{-2} respectively. The ratios [O I(63)/C II(15 8)] / [O I(63)/O I(145)] are thus 1.97/12.5, which are typical of a PDR illuminated by a radiation field of intensity $\sim$ 3 10^4 G_o and $n(H_2)\sim$ 10^4 cm^{-3} (Nisini *et al.* 1996). From the SWS ice features, we derive the following column densities for *solid phase material*; H_2O: 3.5 10^{17} cm^{-2}, CO: 1.25 10^{17} cm^{-2} and CO_2: 1.2 10^{17} cm^{-2}, following Whittet *et al.* (1996). The optical depth of the H_2O line is $\sim$ 0.13, corresponding to a visual extinction $A_v \sim 5$ magnitudes, and the silicate absorption features originate at $A_v \sim 15$ magnitudes, representing the different evaporation conditions at the grain surfaces of the respective species.

We have modelled the SED of the envelope of M8E in order to get information about the circumstellar material that surrounds the object. The model consists of a spherical dust envelope with a radius R_{ext} in which the temperature T and density ρ vary according to power laws, with exponents p and q, respectively:

$$T(r) = T_{ext}\left(\frac{R_{ext}}{r}\right)^p \;\; ; \;\; \rho(r) = \rho_{ext}\left(\frac{R_{ext}}{r}\right)^q, \;\; (p, q > 0)$$

Each point in the envelope is considered to emit as a greybody and then the emission is extinguished along the path traveled through the envelope. The

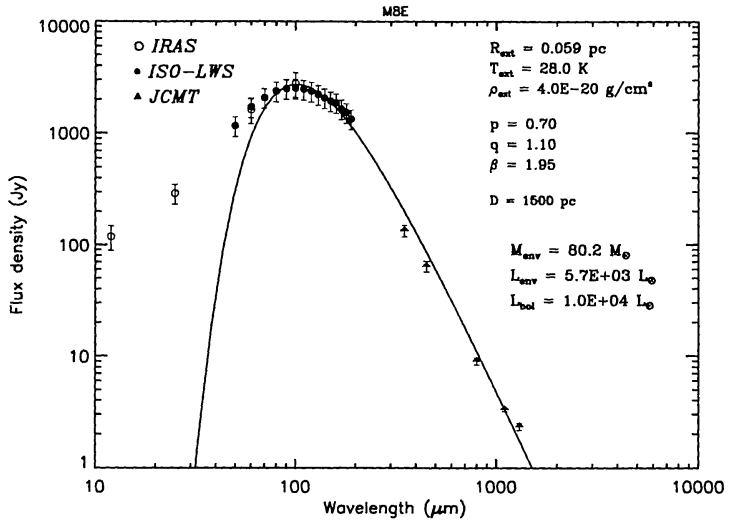

Figure 4. Spectral energy distribution and modeling for the M8E envelope. The (sub)-millimeter data are unpublished data obtained at the JCMT in March 1995. The LWS data, corrected for "off-source" emission, were binned into 15 points for ease of modeling.

total emission coming from the envelope is computed by considering several lines of sight and then integrating along the envelope. Figure 4 shows the spectral energy distribution of M8E using IRAS-PSC data (open circles), LWS data (filled dots) and unpublished JCMT data (filled triangles), together with the line curve obtained from the modeling. The best agreement with the data is obtained with the parameters R_{ext} = 0.059 pc, $\rho_{ext} = 4.0\times10^{-20}$ g cm^{-3}, T_{ext} = 28 K, $p = 0.7$, $q = 1.1$ and $\beta = 1.95$ (β is the opacity law coefficient). The radius of the envelope R_{ext} = 0.059 pc corresponds to $\simeq 16''$ at the distance of 1500 pc. This means that the radius of the envelope is a significant fraction of the JCMT 19″ beam. In fact, from the radial emission distribution predicted by the model we estimate that 12% of the emission from the envelope should be lost by the JCMT beam as a consequence of our single point photometry. For this reason we corrected the JCMT fluxes upwards by 12%. From the figure we can see that the model agrees reasonably well with the (sub)-millimeter data as well as with the LWS data ranging from $\simeq$ 80–200 μm. We note however that the situation may be more complex if there are substantial temperature and density gradients, resulting in different material being contained within the differing beam diameters at each wavelength.

The model fails to reproduce the emission at the shorter wavelengths but this is expected because the spherical envelope description is not totally realistic. In fact, the short wave end of the spectrum, as well as the bolometric luminosity of M8E can be reasonably well fitted with a B0 star surrounded by a 1.2 $M_\odot$ circumstellar disk, inclined about 75 degrees from the plane of the sky, in addition to the envelope described above. Further discussion of this disk modeling will be deferred to a later paper. Considering a distance of 1500 pc we derived an envelope mass associated to M8E by integrating the density distribution along the envelope, obtaining a value for M_{env} = 80 $M_\odot$. Integrating the emission under the model we estimate an envelope luminosity of 5.7×10^3 $L_\odot$

and integrating under the observed spectrum from 12 μm to 1300 μm we derive a bolometric luminosity of $L_{bol} = 1.0 \times 10^4$ $L_\odot$.

3. Conclusions

An $\sim$ 1500 $M_\odot$ molecular cloud surrounds the optically prominent Lagoon Nebula, M8. The outer parts of the cloud contain shells of material, along the edges of which there appears to be triggered star formation. Intense CO line emission is found close to a $\sim 0.2 \times 0.3$ pc, $\sim$ 31 $M_\odot$ molecular core coincident with H 36. Based on the ratios of IRAS fluxes (not shown here) this has a dust temperature $\sim$ 55 K and luminosity $\sim$ 20,000 $L_\odot$. M8E is the second brightest far-IR source in the Lagoon Nebula. It has a temperature $\sim$ 28 K and luminosity $\sim 10^4$ $L_\odot$. An analysis of the ISO LWS lines, and comparison with a nearby 'off-source' reference spectrum suggests that most of the emission lines are typical of a PDR illuminated by a radiation field of intensity $\sim 3\ 10^4$ G_o and $n(H_2) \sim 10^4$ cm^{-3}, and for the ice features, we derive the following column densities for *solid phase material*; H_2O: 3.5 10^{17} cm^{-2}, CO: 1.25 10^{17} cm^{-2} and CO_2: 1.2 10^{17} cm^{-2}. The optical depth of the H_2O line is $\sim$ 0.13, corresponding to a visual extinction $A_v \sim 5$ magnitudes, and the silicate absorption features originate at $A_v \sim 15$ magnitudes, representing the different evaporation conditions at the grain surfaces of the respective species.

4. Acknowledgements

We acknowledge the provision of image processing computer equipment provided as part of a Royal Society grant. The K′ frame is archival data from the Anglo Australian Telescope, taken by Dr David Allen, and kindly made available by Dr David Malin. The JCMT is operated by the JAC on behalf of PPARC, NWO and the NRC.

References

Beckwith, S., Persson, S.E., Neugebauer, G., Becklin, E.E. 1978, ApJ, 223, 464.

Brand, P.W.J.L., Moorhouse, A., Burton, M.G., Geballe, T.R., Bird, M., Wade, R. 1988, ApJ, 334, L103.

Dyck, H.M. 1977, AJ, 82, 129.

Elliot, K.H., Goudis, C., Hippelein. H., Meaburn, J. 1984, A&A, 138, 451.

Gautier, T.N., Fink, U., Treffers, R.R. Larson, H.P. 1976, ApJ, 207, L129.

Lada, C.J., Gull, T.R., Gottlieb, C.A., Gottlieb, E.W. 1976, ApJ, 203, 159.

Nisini *et al.* , 1996, A&A, L321, 315.

Stecklum, B., Henning, T., Eckart, A., Howell, R.R., Hoare, M.G. 1995, ApJ, 445, L153.

White, G.J., Padman, R. 1991, Nature, 354, 511.

White, G.J., Sandell, G. 1995 A&A, 299, 179.

White, G.J., Tothill, N.F.T., Matthews, H.E., McCutcheon, W.H., Huldtgren, M., McCaughrean, M.J. 1997 A&A, 323,529.

Whittet, D.C.B. *et al.* , 1997 A&A, L357, 315.

Woodward, C.E., Pipher, J.L., Helfer, H.L., Sharpless, S., Moneti, A., Kozikwski, D., Oliveri, M., Willner, S.P., Lacasse, M.G., Herter, T. 1986, AJ, 91, 870.

Woodward, C.E., Pipher, J.L., Helfer, H.L., Forrest, W.J. 1990, ApJ, 365, 252.